

ENHANCEMENT OF AN AIRCRAFT DESIGN ENVIRONMENT FOR THE DESIGN OF FIGHTER AIRCRAFT

M. A. C. Hasenau*, S. A. Varga*, A. E. Scholz*, M. Hornung*

* Institute of Aircraft Design, Technical University of Munich, Boltzmannstraße 15, 85748 Garching, Germany

Abstract

A specialized field of aircraft development is the design of high-performance military fighter jets. This paper outlines the steps undertaken to enhance an existing aircraft design environment using a central data model as a single data source for the conceptual design of fighter aircraft. New design challenges were, among others, the approximation of the aerodynamic and geometrical effects of supersonic flight and increased manoeuvrability requirements, with the latter requiring the implementation of negative stability values during horizontal tail sizing. The introduced enhancements are specifically valid for fighter aircraft, such as e.g. the mission fuel mass and component mass estimations, and addressing low aspect ratio wings and their aerodynamic properties. The aerodynamic calculations were undertaken using handbook methods for the preliminary estimation of non-linear lift. The design process was validated with the re-design of the F-16A Block 15 fighter aircraft. With the implemented methods, the reference aircraft's wing loading and thrust-to-weight ratio are closely matched. As a result, the F-16A re-design's maximum take-off weight and wing reference area are nearly identical to the reference fighter aircraft. This applies to the mass breakdown and geometrical dimensions as well. The implemented fighter aircraft design process therefore proved to lead to reasonable results.

Keywords

aircraft design; fighter aircraft; panel codes; non-linear aerodynamics

NOMENCLATURE

Symbols

α	angle of attack
β	sideslip angle
Δ	delta
η	efficiency
Λ	sweep
λ	taper ratio
\bar{x}	normalized distance
σ	static margin
AR	aspect ratio
b	wing span
BPR	bypass ratio
C	coefficient
c	chord length
E	energy exchange
e	Oswald span efficiency factor
K	factor
k	drag-due-to-lift factor
MLM	maximum landing mass
MTOM	maximum take-off mass
MTOW	maximum take-off weight
n	load factor
q	dynamic pressure
S	wing surface
TSFC	thrust specific fuel consumption
WDF	wave drag factor
y	length unit

Indices

50	50% chord line
0	sea level
deg	afterburner
deg	aerodynamic centre
AB	average
AC	break
-	span
av	center of gravity
B	critical
o	cranked wing
b	zero-lift drag
-	drag
CG	lift induced drag
cr	fuselage
cw	high-lift device
-	horizontal tail
D0	inner
D	leading edge
-	linear
Di	lift
fus	maneuvering
HLD	maximum
HT	nose
i	outer
-	plain flap
LE	reference
lin	required
L	root
man	
max	
nose	
o	
plain	
ref	
req	
r	

sub	subsonic
super	supersonic
TR	thrust reversal
t	tip
ult	ultimate load
V	vortex
wave	wave
wet	wetted
wing	wing
WME	wing mass estimation
z	z-direction

Abbreviations

AAA	Advanced Aircraft Analysis (Software)
ADEBO	Aircraft Design Box (Software)
ATR	Attained Turn Rate
CG	Center of Gravity
FADS	Fighter Aircraft Design System (Software)
FCAS	Future Combat Air System
ICL	Iterative Calculation Loop
KEACDE	Knowledge-based and Extensible Aircraft Conceptual Design Environment (Software)
METU	Middle East Technical University
NACA	National Advisory Committee for Aeronautics
NAWBPP	NASA Ames Wing-Body Panel Program (Software)
OEM	Operating Empty Mass
OpenVSP	Open Vehicle Sketch Pad (Software)
PANAIIR	Panel Aerodynamics (Software)
RDS	Raymer's Design System (Software)
SFC	Specific Fuel Consumption
STR	Sustained Turn Rate
TSFC	Thrust Specific Fuel Consumption
TU	Technical University
UAV	Unmanned Aerial Vehicle
WDF	Wave Drag Factor

1. INTRODUCTION

During the increasingly complex design process of an aircraft, a small change in the design parameters can result in the alteration of the overall result. Consequently, it is becoming common to design new aircraft with different computer-based software to exploit rapid estimation capabilities. This way it is a relatively low effort and high reward task to investigate the effects of parameter variations. For the conceptual and/or preliminary design stages, several aircraft design software solutions are available for purchase or in freeware form. Unfortunately, none of the freeware design environments is capable of designing air force fighter aircraft and has an editable source code enabling modifications of the underlying functions as required for scientific exploration of the topic.

The main objective of this work is therefore to extend the capabilities of the Technical University of Munich Institute of Aircraft Design in-house aircraft design environment Aircraft Design Box (ADEBO) to air force fighter aircraft design. The focus will be set on the capabilities to re-design aircraft similar to the F-16 fighter aircraft

(fourth generation fighter). This will lie the foundation for future studies regarding a sixth generation fighter aircraft. Especially in view of the plans of France, Spain and Germany concerning a Future Combat Air System (FCAS) this is indispensable. Furthermore, in the long term, it is planned to incorporate ADEBO into teaching at TU Munich, such that students attending the "High Performance Aircraft" lecture will benefit from this fighter design extension of ADEBO.

In the following, first, a review of existing fighter aircraft design environments is provided. Second, ADEBO and the methods and process for fighter design implemented are described in depth. Third, the results of the design process are presented and subsequently discussed. Finally, a conclusion is drawn and areas for future work are identified.

2. REVIEW OF EXISTING FIGHTER DESIGN ENVIRONMENTS

Several existing aircraft design environments that can be used for the conceptual design of fighter aircraft have been identified by the authors. They will be presented briefly in this section to provide an overview of previous work in the field.

2.1. Raymer's Design System

An example of a commercially developed aircraft design environment is Raymer's Design System RDS-Professional [1]. It is capable of designing fighter aircraft as well as general aviation and civil transport aircraft and was developed by Daniel P. Raymer. Its core capabilities are: the analysis of aerodynamics, stability, mass, propulsion, cost, performance, and range. The program can be considered as a complement to Raymer's aircraft design book [2], despite having evolved from an instructional aide to a full fledged aircraft design environment.

2.2. Advanced Aircraft Analysis

The Advanced Aircraft Analysis (AAA) software by the DARcorporation was originally based on the aircraft design methods provided in the books series by Roskam "Airplane Design", but has evolved since then. It can be used for the conceptual and preliminary design of most fixed wing aircraft. Specialised methods for the design of fighter aircraft (e.g. weight module and the drag module applicable to the supersonic flight regime) allow the design of such type of aircraft. Among others, modules for weight and balance, aerodynamics, stability and control, performance, and cost estimations are provided. A drawback for the fighter design, is that the stability and control derivatives can only be calculated for subsonic flight regimes. [3]

2.3. Fighter Aircraft Design System

The Fighter Aircraft Design System (FADS) was developed by the Institute for Defense Analyses as part of a contract with the US Government issued in 1988. It is

fairly unique in the sense that it was not adapted from an existing design environment capable of designing civil aircraft, but developed from the beginning to design military aircraft. It includes four major aircraft design stages: 1) the fighter sizing model, 2) the range-payload model, 3) the energy/maneuverability model, and 4) the cost estimation model. Significant drawbacks of this software tool are its inability to design supersonic military aircraft and its limitation to designing aircraft in the MTOM range from 2268 *kg* to 22680 *kg*. [4]

2.4. Naval Postgraduate School Course Assisting Program

The conceptual design program developed by Michael Cramer as part of his Master's thesis was developed specifically to be used in the Naval Postgraduate School's Department of Aeronautics to support the lecture specializing in fighter and attack aircraft design. The target audience were students that were already familiarized with handbook methods for conceptual design. By using the program, students were guided through the steps of aircraft design, while eliminating the need to calculate every equation by hand. To prevent the program from becoming a black box, it was programmed not to be over automated and to enable the student, to follow the logical sequence of program steps. [5]

2.5. Middle East Technical University's Fighter Design Process

The Middle East Technical University's (METU) fighter design process is an example for an university-created computer aided design method and was developed by Mert Tokel [6]. Its intention is to analyze the effects of initial engine scaling on fighter conceptual design by using a competitor aircraft's aerodynamic characteristics as reference. As sources for the design mission and requirements for the validation of the design process, Tokel used [7] and [8]. Interesting methods that are utilized in this design environment are the interface to the software OpenVSP for a parametric external fuselage surface definition depending on defined internal components, and the method presented in [8] for the influence estimation of initial engine selection on fighter design processes. [6]

2.6. Knowledge-Based and Extensible Aircraft Conceptual Design Environment

A design environment that has similarities to ADEBO, is the Knowledge-Based and Extensible Aircraft Conceptual Design Environment (KEACDE) developed by the Ministry of Industry and Information Technology in China. It is capable of designing civil as well as military aircraft, and utilizes a two level architecture: On the top level, experienced engineers can create software tool bundles that can be utilized by inexperienced designers on the lower level. The capabilities of the KEACDE software are further enhanced by its ability to use third party software, like PANAIR, to account for capabilities not implemented in the basic suite. [9]

3. METHODS

In this section, the in-house aircraft design environment ADEBO is presented, as well as the methods implemented to extend ADEBO for fighter aircraft design.

3.1. Aircraft Design Environment ADEBO

At the Institute of Aircraft Design of the Technical University of Munich, the aircraft design environment ADEBO, is under development for the application in research and teaching. In contrast to commercially available design environments, the requirements for ADEBO were, among others, the possibility to use various tools of different fidelity, the utilization of already existing software with uniform application procedures, and consequently a central data model as a single data source. ADEBO is implemented using the MATLAB platform and offers high flexibility and extensibility due to its modular structure. Likewise, the central data model is implemented with an object-oriented structure to ensure code re-usability, scalability, modularity, and easy maintainability. Currently, various types of conceptual and early preliminary fixed-wing subsonic aircraft can be designed within ADEBO: kerosene-, battery-, and hydrogen-powered subsonic transport aircraft (short-, medium-, and long-range), and small unmanned aerial vehicles (UAVs). For more information about ADEBO, the reader is referred to [10].

3.2. Fighter Design in ADEBO

In order to initiate an aircraft design in ADEBO, precise requirements regarding the aircraft performance and the executable mission profile have to be defined. In case of the performance requirements, values for the required stall speed, and the runway length for both the take-off and landing have to be specified. Other performance values like the attained and sustained turn rates, the available specific excess power, and of course the requirement toward the maximum Mach number has to be described as well. In general, the fighter is expected to fly with both subsonic and supersonic Mach numbers. Furthermore, with respect to the flown mission, the aircraft is expected to perform a mission either with returning to the origin base or to an alternative airfield. Additionally, via a sudden drop of payload, it is possible to simulate the effect of armament deployment on the overall design process. Based on the estimation method for the fuel mass that is required for the prescribed mission, it is possible to build-up the flight profile by a user-defined number of segments for cruise, loiter, climbing and ascending. Nevertheless, the total climbed height must equal the total altitude loss during descending.

To execute the design process's first step, initial estimations must be made for the aircraft's wing and tail aspect ratio, taper ratio and sweep angle, for the maximum take-off weight and the achievable maximum lift coefficient. These values are mostly taken from statistical charts or are estimated with the help of already existing and similar aircraft configurations. The overall design process

executes individual calculations subsequently and with iterative calculation loops (ICLs) (Gauss-Seidel method). An overview of this process is given in FIGURE 1. In the following sections, the implemented design steps are explained in detail.

3.2.1. Design Step: Basic Aerodynamics

Most current in-service fighter aircraft, and most likely future ones as well, perform missions not only in the subsonic regime, but at supersonic speeds as well. This supersonic flight regime has to be adequately addressed during the design process. One of the most significant effects is the increase of the zero-lift drag due to shock wave development around the aircraft's body. When executing the *Basic Aerodynamics* step, the output values are the zero-lift drag, the initial lift curve slope and induced drag coefficient, the critical Mach number, and the Oswald span efficiency factor. All these values are direct input into the following design step, the *Point Performance*.

To calculate the subsonic zero-lift drag, for a first assumption the product of the overall wetted surface to wing reference area ratio $\frac{S_{wet}}{S_{ref}}$ and the equivalent skin friction coefficient C_{fe} is estimated. The equivalent skin friction coefficient might be approximated as 0.0035 after Raymer [2]. This is a statistically estimated value especially for fighters. In the absence of any geometry during the first stages of the design process, the exact value of the wetted surface ratio is not known. Thus, a statistical equation has been developed. Several aircraft with similar characteristics were selected and a relationship based on their maximum take-off weight was made:

$$(1) \quad \frac{S_{wet}}{S_{ref}} = 0.03 \cdot MTOM[t] + 3.658$$

In the following step, the critical Mach number has to be calculated since this is required to accurately determine the zero-lift drag and consequently the overall drag polar. This critical Mach number estimation is based on Raymer [2]. The equation is especially used for NACA 6-series airfoil and is credible for supercritical profiles as well.

The airfoil profile thickness is estimated relying on the historical trend line found in [2].

Again, in the absence of any geometry or volumetric distribution, it is not possible to precisely calculate the wave drag at this early phase of the design. Similarly to the wetted surface ratio, a number of fighter aircraft with known drag polars for the supersonic flight regime were found. These were gathered, and as a result of an analysis, a relationship between these polars could be established [11]. Based on this relationship, it is possible to identify a wave drag factor (WDF):

$$(2) \quad C_{D0_{sup}} = C_{D0_{sub}} \cdot WDF$$

Regarding the above-mentioned fighter database compilation, prerequisites were that Withcomb's transonic area rule was known before their design date, that the aircraft

are capable of supersonic flight, and that these aircraft had NACA airfoils with similarly low thickness-to-chord ratios. Finally, the wave drag factor as a function of the aspect ratio is estimated as:

$$(3) \quad WDF = 0.333 \cdot AR^2 - 1.66 \cdot AR + 4.112$$

As the calculation of the lift-curve slope C_{L_α} is driven by the lifting surface's aspect ratio and the flight Mach number, different methods had to be implemented. For aircraft with wing aspect ratios lower than 2, the C_{L_α} is estimated with the Slender Body Theory throughout the entire flight velocity range:

$$(4) \quad C_{L_\alpha} = \frac{\pi \cdot AR}{2}$$

In contrast to this, if a wing with an aspect ratio greater than 2 is used, the subsonic C_{L_α} is estimated with the Polhamus Theory:

$$(5) \quad C_{L_\alpha} = \frac{2 \cdot \pi \cdot AR}{2 + \sqrt{\frac{AR^2 \cdot (1 - Ma^2)}{\eta^2} \cdot \left(1 + \frac{\tan^2 \Lambda_{50}}{1 - Ma^2}\right)} + 4}$$

where for the conceptual phase the airfoil efficiency η might be approximated with 0.95. If a supersonic leading edge is present, C_{L_α} is estimated by the Ackeret Method:

$$(6) \quad C_{L_\alpha} = \frac{4}{\sqrt{Ma^2 - 1}}$$

Finally, the Oswald span efficiency factor e is calculated. This allows to take into account the non-elliptical lift distribution. Since this factor is depending on the wing's sweep angle, the equations from Raymer [2] based on actual aircraft are implemented. They distinguish between wing sweeps lower or higher than 30°.

3.2.2. Design Step: Point Performance

After the *Basic Aerodynamics* step, the required wing reference area S_{ref} and the engine sea level thrust T_0 are calculated. This is done using the design chart: a diagram where the horizontal axis represents the wing loading $MTOW/S_{ref}$ and the vertical axis the thrust-to-weight ratio or thrust loading $T_0/MTOW$.

The wing loading and the thrust loading are both directly affected by point performance requirements such as specific excess power and maximum flight speed. These performance values govern the limiting equations used in the design chart.

The curves of these limiting equations in the design chart will leave the designer with an acceptable region where any selected thrust loading and wing loading pair satisfies all the determined aircraft performance requirements. Commonly in the acceptable region - as in this fighter design as well - a design point with the smallest thrust

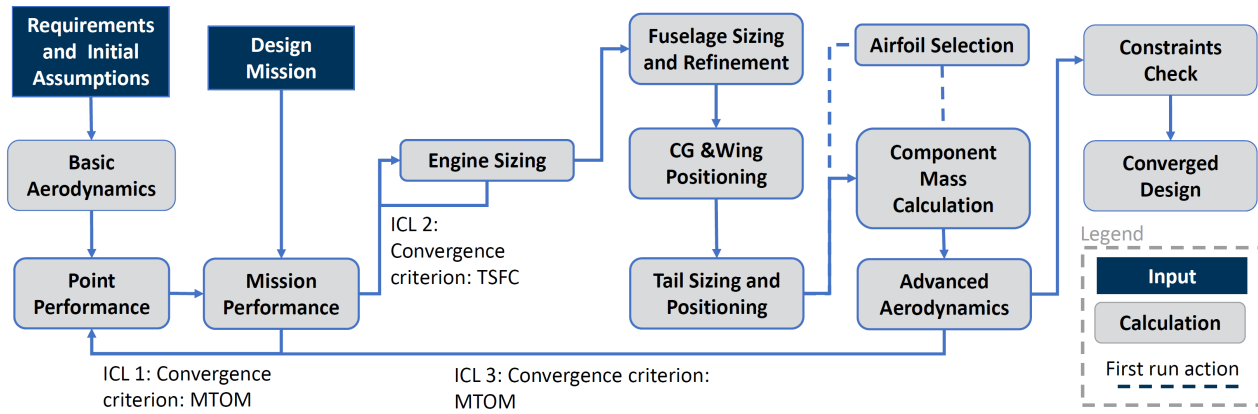


FIGURE 1. Fighter aircraft design process within ADEBO

loading is used as this results in the smallest acceptable engine size. This in turn reduces the aircraft's unit cost. With the initially estimated maximum take-off mass it is then possible to determine the wing reference area S_{ref} and the engine sea level thrust T_0 .

When no exact stall speed value is prescribed in the initial specifications, then after Sadraey [12] for a fighter with supersonic flight capability, the approximate value of $50 - 60 \frac{m}{s}$ is used. The stall speed and landing distance limiting equation solely influence the wing loading of the design. Further limiting equations affecting both the thrust loading and the surface loading are the maximum flight speed, the take-off and landing runway length, and the requirements towards the achievable rate-of-climb and turn rates.

When prescribing the maximum flight speed at a given altitude, it is assumed that for the longitudinally trimmed aircraft the aircraft drag is balanced by the engine thrust and that the aircraft is in horizontal flight, thus the vehicle weight is counteracted by the generated lift. When a fighter with supersonic flight capability is designed, then different zero-lift drag coefficient and different drag-due-to-lift factor are used for sub- or supersonic flight conditions.

In case of the runway length requirements, next to the aerodynamic coefficients like achievable maximum lift or total zero lift drag, inputs such as runway surface friction coefficient or average deceleration coefficient are required as well. The latter, especially in the early stage of design might be assumed as $1.9m/s^2$ when using a simplified brake system, while for fighters equipped with airbrakes a value of $3.9m/s^2$ can be applied, with values taken from [13]. It is noted that in the implemented limiting equation for take-off runway length requirement the total field length is the take-off acceleration runway length only, which is the length required to accelerate the fighter to take-off speed.

Another essential performance measure for a fighter is the achievable rate-of-climb or specific excess power. Generally, in the specifications requirements, the specific excess power is defined together with the corresponding flight altitude, the manoeuvring weight, and the Mach number. In the uncommon case that the specific excess power is

given for supersonic flight speeds, the aerodynamic coefficients have to be adjusted to this condition.

Finally, to describe the manoeuvring capability of the fighter, the achievable turn rates have to be addressed as well. It is differentiated between the sustained turn rate STR and the attained turn rate ATR. When the aircraft performs a turn at its sustained turn rate, no accountable loss of altitude or loss of flight velocity is present., and the limiting equation is mainly driven by the manoeuvring load factor n_{man} . In contrast to this, the attained turn rate is driven by the achievable maximum lift coefficient $C_{L_{max,man}}$.

3.2.3. Design Step: Mission Performance

As fighter aircraft must meet strict mission requirements like endurance, ammunition type and weight carried on board, or cruise Mach number, it is vital to predict the minimum aircraft weight and the fuel weight to accomplish a required flight profile.

For the fuel mass estimation, the method introduced by Roskam [14] has been used. The results are the gross take-off weight, the aircraft empty weight, and the fuel weight required for the predefined mission. Prior to the fuel mass estimation, the following mission parameters have to be specified: payload weight and its influence on zero-lift drag, required range, altitude and flight speed during cruise and manoeuvring, and the loiter and manoeuvre endurance.

With the breakdown of the entire flight mission into different phases and by using experience-based fighter specific fuel fractions for these, it is possible to determine the overall required fuel weight. A fuel fraction is the ratio of the end-weight and start-weight of the corresponding flight phase. In contrast to flight phases such as engine start, take-off, or taxiing, the calculations of the fuel mass fraction for the cruise, manoeuvre and loiter phases are based on the Breguet equations for range and endurance. The calculations of the latter mentioned phases also include considerations concerning the payload drop (armament usage) and the increase of zero-lift drag due to mounting external payload on the wing and fuselage. This zero-lift drag increase was estimated according to [2].

For the empty weight estimation in the first iterations, a method based on the relationship by the Wright Laboratory [15] was implemented. This is specifically established for supersonic fighters and describes the increase of maximum take-off weight with the increasing product of payload weight and required range. This resulting initial take-off gross weight is then inserted in Raymer's empirical empty weight estimation for fighter aircraft. Following the *Mission Performance* design step, the value of the maximum take-off mass is updated. If this resulting new maximum take-off weight shows a difference to its originally assumed value greater than a specified delta, then consequently the first iteration loop is started. During this, the *Point Performance* and *Mission Performance* calculation steps are executed until the resulting delta is less than its specified value.

3.2.4. Design Step: Engine Sizing

To determine the geometrical, mass, and performance properties of the installed engine, the equation system by Raymer [2] was used. The equations distinguish between non-afterburning engines and afterburning engines. For both distinguished equation systems, the required inputs are the bypass ratio, the required sea level static thrust, and the achievable maximum Mach number. In case of the sea level thrust, it is an input value derived from the *Point Performance* step. This thrust value is equally split among the number of engines.

In general, the *Engine Sizing* step results in the fighter aircraft engine's diameter, length, mass, and the thrust specific fuel consumption (TSFC). The implemented equations have a restriction towards the engine's bypass ratio, namely from zero up to one. The maximum Mach number has to be less than 2.5. In case of engines designed after the year 1995, an additional mass, length, and TSFC reduction of 20% is suggested.

Currently, the *Engine Sizing* design schedule is closed by the second iteration loop as the resulting TSFC is compared with its initially assumed value. Assuming that the new TSFC is higher than the TSFC value used as an input during the previous *Mission Performance* design step, the engine bypass ratio is increased. Consequently, beginning from the *Point Performance* step, all the previous calculations are initialized again with the new bypass ratio. This iteration loop runs until the resulting TSFC is lower or equals the input TSFC from the initial assumptions.

3.2.5. Design Step: Fuselage Sizing and Refinement

In the *Fuselage Sizing and Refinement* step, the fuselage length and diameter as well as the cockpit dimensions are estimated. The fuselage length is calculated according to an empirical function postulated by Raymer [2], which depends on the MTOM of the aircraft configuration:

$$(7) \quad l_{fus} = 0.93 \cdot (MTOM \cdot 2.2046)^{0.39} \cdot 0.38$$

The above equation results in greater fuselage length values than military aircraft have. To deal with this problem, a study was conducted with 13 similar fighter aircraft. The average difference between the actual and the Raymer-based calculation resulted in 15.5% additional length [11]. Hence, the equation from Raymer is multiplied by a factor of 0.845 to match existing fighter aircraft designs.

An average fuselage diameter in the nose section of fourth generation fighter aircraft was estimated by Varga to be $d_{nose,av} = 1.21 \text{ m}$ [11] and used within this study. The diameter of the nose section is set to equal this average diameter, to account for the body size of a fighter pilot and the necessary cockpit instrumentation. In case the engine(s) have a larger diameter than the fuselage diameter incorporating the engine(s), the tail section's diameter is set to be the engine(s) diameter. The transitions between the fuselage sections with different diameters are designed to have a maximum inclination angle of 12° , as suggested by [2], to prevent airflow separation.

To get an estimate of the cockpit diameter and length, the general fighter cockpit layout shown in [2] has been chosen for implementation. In case of a two-seater configuration, the cockpit length is doubled.

3.2.6. Design Step: Centre of Gravity and Wing Positioning

Following the *Fuselage Sizing and Refinement* design step determining the initial fuselage geometry, the location of the wing is calculated. When initiating the design process of ADEBO for the first time, only the fuel and the payload masses are known and they are used as reference weight for the wing position calculation. After the component masses of the wing and fuselage have been estimated in the *Component Mass Estimation* design step later on, the position calculation includes their masses as part of the third iterative calculation loop. For this design step, the center of gravity of the fuselage and the wing is calculated separately. In ADEBO's fighter design schedule, the determination of the center of gravity is conducted using the OpenVSP software by NASA. The relationship of the overall center of gravity with respect to the wing aerodynamic chord is as follows:

$$(8) \quad \bar{x}_{CG_{wing,fus}} = \bar{x}_{AC_{wing}} - \sigma$$

where the σ describes the static margin of the aircraft configuration and the dash above the distances x denotes that these distances are normalized by the mean aerodynamic chord. Since fighters have highly swept wings and operate with high Mach numbers, the estimation of the aerodynamic center is done with respect to the wing apex [16].

3.2.7. Design Step: Tail Sizing and Positioning

The calculation of the vertical and horizontal tail and the related longitudinal and directional stability analysis is done separately. This is possible, since aircraft are mostly symmetrical with respect to their longitudinal axis, thus

the coupled effect of angle of attack disturbance on yaw and roll movement can be neglected [2]. Furthermore, modern fighter aircraft are often designed to be longitudinally unstable, meaning that when disturbed, the aircraft will not automatically return to its original orientation, but changes its pitch. The calculation with such a negative static margin is implemented in the horizontal tail calculation.

Horizontal Tail Sizing

The calculation of the area of the horizontal tail is related to the longitudinal static stability requirement. Per definition, in a trimmed flight state around the aircraft's center of gravity, the overall pitching moment must be zero [2]. For static trim, two different cases are analysed. First, during the take-off phase when the aircraft reaches its highest achievable lift coefficient and consequently a high pitching moment. Second, during flight with supersonic Mach number. For a supersonic condition, the aerodynamic center will be shifted back up to 50% of the chord length. Consequently, for an adequate horizontal tail sizing this shift has to be calculated. This is done by the method described in DATCOM [17] and is valid at every flight speed and for several wing taper ratios and aspect ratios.

For longitudinal stability, the most aft center of gravity position is critical. Two different scenarios are analysed; either the overall amount of fuel is burned, or the aircraft deployed all its payload. If the payload and fuel are not assumed to be at the same location as the center of gravity, setting these masses to zero results in a shift of the center of gravity. Whichever results in the most aft center of gravity position, is used in the later calculations. The moment equation around the most-aft center of gravity position is implemented as:

$$(9) \quad \frac{S_{HT}}{S_{ref}} = \frac{C_{L_{\alpha W}}}{C_{L_{\alpha HT}}} \cdot \frac{d\alpha}{d\alpha_{HT}} \cdot \frac{q}{q_{HT}} \cdot \frac{\bar{x}_{CG} + \sigma - \bar{x}_{AC_{wing}}}{(\bar{x}_{AC_{HT}} - \bar{x}_{AC_{wing}}) - \bar{x}_{CG} - \sigma + \bar{x}_{AC_{wing}}}$$

In the final calculation step, the distance between the horizontal tail aerodynamic center and wing aerodynamic center is increased until the horizontal tail's trailing edge reaches the end of the fuselage. This way the lowest possible horizontal tail area acts on the longest possible tail moment arm.

Vertical Tail Sizing

Although in the lateral-directional analysis the yaw and the roll movement are coupled, both depend on the yaw or side-slip angle β . As a result of this, for the preliminary stage, the vertical tail area is calculated by using the yaw moment derivative $C_{N_{\beta}}$. A historical trend-line is found in NASA's Technical Note D-423 as cited by Raymer [2], where a relationship between the flight Mach number and

the $C_{N_{\beta}}$ value is presented. By the selection of a $C_{N_{\beta}}$ value, it is then possible to calculate the vertical tail area. Similarly to the horizontal tail, the same flight phases affect the vertical tail's area, namely the take-off and the flight with maximum Mach number. Again, the resulting higher value for the vertical tail area is carried on for successive calculations.

3.2.8. Design Step: Airfoil Selection

For the selection of the airfoil, a method was introduced that considers the effects of a supersonic cruise flight regime on airfoil selection. Based on the wing sweep and cruise Mach number, it is determined whether the leading edge of the wing is outside the Mach cone. If the leading edge lies outside, the process advises selecting a supersonic airfoil (e.g. a thin airfoil or a double-wedge airfoil). In contrast to this, if the leading edge is inside the mach cone, the method of Sadreay is used for airfoil selection [12]. The latter is based on a look-up table where with the determination of the required ideal and maximum lift coefficients, a NACA airfoil is selected.

3.2.9. Design Step: Component Mass Estimation

To estimate the Operating Empty Mass (OEM), the different component masses of the structure group, propulsion group, and the fixed masses are estimated and combined to form the new OEM. The component mass estimation of fighter aircraft and civil transport aircraft differs greatly, therefore different methods had to be implemented, which are presented in this subsection. Where applicable, component mass fudge factors have been utilized, which can be found in [2].

The structure mass contains the masses of the following components: wing, horizontal tail, vertical tail, fuselage, landing gear. For the wing mass estimation, the method of the Luftfahrttechnisches Handbuch [18] was chosen and adapted for the use on cranked wing fighter aircraft. The results were validated using the F-16A and F-18A wing masses as reference. A basic difference is the use of the whole wing area of the cranked wing as reference area for this calculation. Furthermore the modifications resulted in the following correction factors to be used in this estimation method:

$$(10) \quad F_{W,cw} = 0.211$$

$$(11) \quad \Lambda_{50,cw} = \frac{\Lambda_{50i} + \Lambda_{50o}}{2}$$

$$(12) \quad S_{ref,WME} = S_{cw}$$

For the estimation of the vertical tail and horizontal tail masses, the methods from [18] were used as well. The mass estimation method of the fuselage structure was undertaken with the method by [18] adopted according to [19]. The landing gear mass is estimated according to an equation from [20].

The combined powerplant mass consists of the following components: engine, air inlet, fuel system, auxiliary power unit, propulsion integration, engine control sys-

tem, and engine starter system. The engine mass calculation was conducted according to formulas for preliminary engine data estimation developed by [2]. The mass estimation of the remaining propulsion components was conducted according to [20].

On top of the component masses of the structure and propulsion, further fixed masses have to be considered. The masses estimated in the fighter design schedule are the following:

- 1) Flight control system
- 2) Oxygen system
- 3) Air conditioning and pressurisation
- 4) Electrical system
- 5) Furnishings
- 6) Instruments
- 7) Gun armament
- 8) Armament

The formulas used for estimating the masses of items 1) to 5) were taken from [20]. The component masses for the instruments and the gun armament were not calculated, as recommended by Roskam [20]: The selected mass for the instrumentation was taken from the actual F-16A aircraft for purpose of the re-design, because Roskam states that one should consult actual instrument weights as his formulas are out of date for aircraft using modern glass cockpits and digital flight management and navigation systems [20]. For the used gun mass, the reference value for the M61A1 Vulcan Gatling gun used in most fourth generation fighter aircraft of the United States found in [20] was chosen. The armament mass was calculated using the method by [18], and incorporates the weapon related items of an aircraft that are not the build-in cannons or that are not considered payload.

3.2.10. Design Step: Advanced Aerodynamics

For the calculation of the aerodynamics of the fighter aircraft, two different methods have been implemented. Each estimates the lift and drag coefficient as well as the lift curve slope at the aircraft's design point. One utilizes the NASA Ames Wing-Body Panel Program (NAWBPP), the first mean aerodynamic panel code that was able to estimate aerodynamic characteristics in a supersonic flight regime. Initially developed under the guide of Frank Woodward in the mid 1960s, it was adapted for use on personal computers by Ralph Carmichael, who was also involved in the programs original development in the mid 1990s. It is available as freeware on the Public Domain Aeronautical Software PDAS website [21] and an interface to ADEBO has been developed.

In modern fighter design non-linear lift phenomena play an important role. For example, fourth generation fighter aircraft like the F-16, F/A-18, Mig-29, and the Su-27, generate vortices at leading edge extensions. These vortices delay the onset of stall enabling higher angles of attack in manoeuvre situations and increase the generated lift in general [22]. The basic wing planform of an aircraft with wing leading edge extensions is called a cranked wing [17]. Due to this cranked wing configuration combined with the consideration of non-linear lift, a refined method has to be adopted for the induced

drag estimation. The second aerodynamic estimation method implemented in the fighter design schedule uses handbook methods based on research done by Polhamus and Staudacher to estimate these non-linear lift effects caused by vortices generated by leading edge extensions of a cranked wing. This second method was used to generate the re-design of the F-16A in this paper and will therefore be presented in more detail in this section.

General Principle of the Method by Polhamus and Staudacher

The calculation of cranked wing lift incorporates aspects of non-linear lift resulting from vortices created by leading edge extensions. The method is based on the assumption that the non-linear lift contribution combined with the linear lift contribution equal the total lift. The non-linear lift contribution is calculated for each wing segment of the cranked wing and weighed by the section's wing area. An example for the cumulative lift coefficient of a cranked wing (cw) with an inner (i) and outer (o) wing segment can be seen in EQUATION 13, which was adapted from [19].

$$C_L = C_{L_{\alpha,lin}} \cdot \alpha + C_{LV,cw,i} \cdot \frac{S_i}{S_{ref}} + C_{LV,cw,o} \cdot \frac{S_o}{S_{ref}} \quad (13)$$

Linear Lift of Cranked Wings and Aerodynamic Center Location

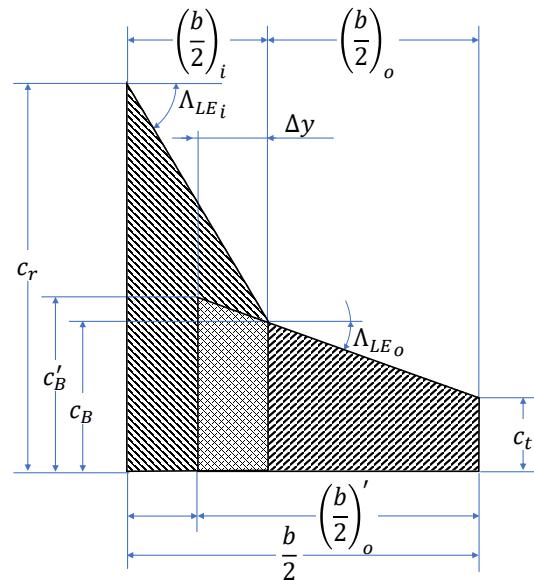


FIGURE 2. Two-section cranked wing

The linear lift component for a cranked wing, as can be seen in FIGURE 2, is calculated according to a method first published by Paniszczyn [23] that was later adapted for Digital DATCOM. It combines handbook methods for the estimation of linear lift of conventional wings with a geometric aspect that represents the cranked

wing planform. As the new wing planform differs from a conventional wing layout, a different method for the aerodynamic center estimation is used that can also be found in [23].

Non-Linear Lift of Cranked Wings

The basis for the implemented calculation of the non-linear lift effects was published by Polhamus [24]. He developed formulas to estimate the non-linear lift effects for certain delta wing configurations. Staudacher adapted the method for use on cranked wing designs. For his method of calculating the non-linear lift of an arbitrary two-section cranked wing, the planform has to be modified to two delta wing sections as can be seen in FIGURE 3. In FIGURE 2 and FIGURE 3 Δy is set to be $\left(\frac{b}{4}\right)_i$.

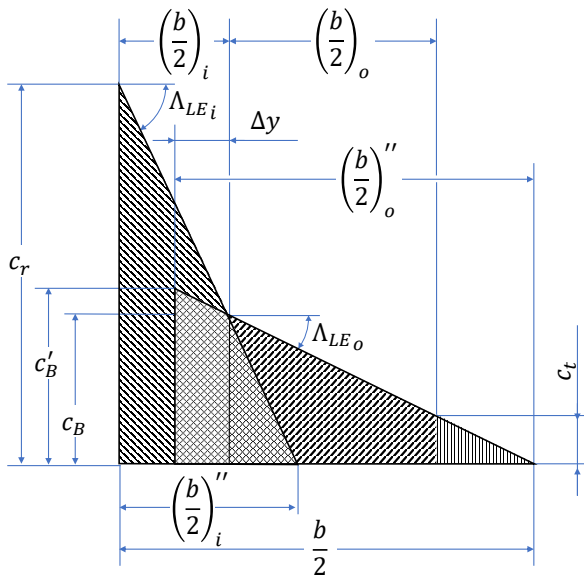


FIGURE 3. Adapted two-section cranked wing

If the resulting delta wing sections are able to create vortices, their influence on the overall lift can be estimated. Criteria for the ability to create vortices are according to Staudacher [22]:

- $\Lambda_{LE} \geq 55^\circ$
- $AR \leq 2.5$
- A sharp leading edge

The vortex-dependent non-linear lift coefficients $C_{LV,i/o}$ are calculated for each wing section as proposed by Polhamus. To estimate their effect on the overall cranked wing lift, the coefficients are multiplied with the wingspan correction factor K_b , as can be seen in EQUATION 14 [19]. The wingspan correction factor can be graphically determined from FIGURE 4. If a wing segment does not fulfill the criteria for vortex creation as listed above, $C_{LV,cw,i/o}$ is set to zero.

$$(14) \quad C_{LV,cw,i/o} = C_{LV,i/o} \cdot K_{b_{i/o}}$$

Induced Drag of Non-Linear Cranked Wings

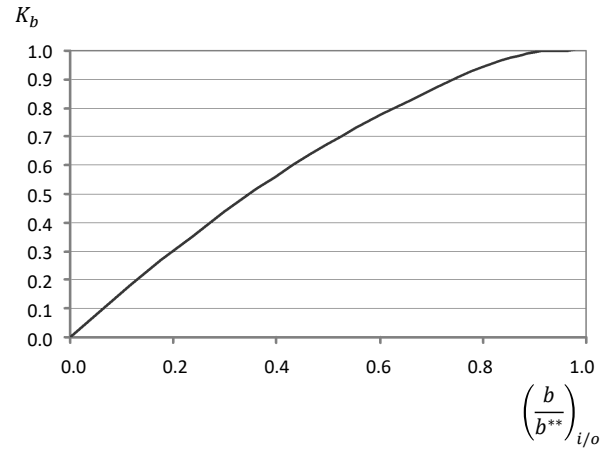


FIGURE 4. Wingspan correction factor K_b as adapted from [19]

For the estimation of the induced drag of cranked wings creating vortices, two scenarios have been investigated by Staudacher. In the first scenario, if both cranked wing sections are able to cause vortices, the lift-induced drag is calculated via EQUATION 18.

For the second scenario, in which only the inner wing is able to cause vortices, a more detailed method has to be applied. For this method, distinct lift coefficients are needed: a critical lift coefficient $C_{L_{cr}}$, and a maximum lift coefficient $C_{L_{max}}$. $C_{L_{cr}}$ is the lift coefficient at which the leading edge suction loss starts to influence the induced drag. For NACA 64-series profiles, it can be estimated as can be seen in EQUATION 15 [22].

$$(15) \quad C_{L_{cr}} = 25 \cdot \left(\frac{t}{c}\right)^{1.6} \cdot \cos^{0.5}(\Lambda_{LE})$$

$C_{L_{max}}$ is the lift coefficient at which the created vortices of the right and left wing begin to influence each other. This coefficient can be graphically determined from FIGURE 5.

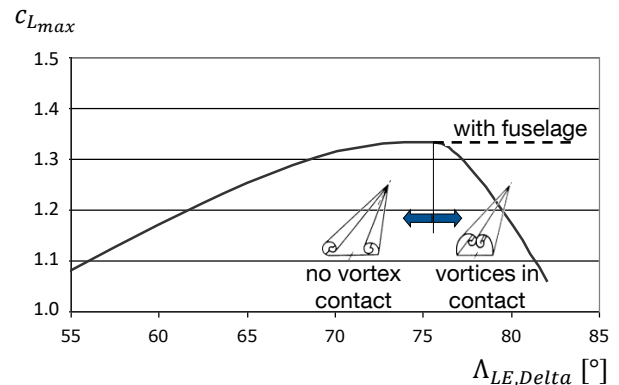


FIGURE 5. Maximum lift coefficient adapted from [19]

With the help of $C_{L_{cr}}$, $C_{L_{max}}$, and the lift coefficient C_L for a certain angle of attack α , three cases can be identified, each requiring a different method of C_{Di} calculation as summarized in TABLE 1.

TABLE 1. Equations for the estimation of the induced drag of vortex generating cranked wings according to [19]

Case	Condition	Equation Nr.
1	$C_L < C_{L_{cr}}$	16
2	$C_{L_{cr}} < C_L \leq 0.75 \cdot C_{L_{max}}$	17
3	$0.75 \cdot C_{L_{max}} < C_L$	18

$$(16) \quad C_{Di} = \frac{1}{\pi \cdot AR \cdot e} \cdot C_L^2$$

$$(17) \quad C_{Di} = \frac{1}{\pi \cdot AR \cdot e} \cdot C_{L_{cr}}^2 + \frac{1}{C_{L_\alpha}} \cdot (C_L^2 - C_{L_{cr}}^2)$$

$$(18) \quad C_{Di} = C_L \cdot \tan(\alpha)$$

Combining the so-calculated induced drag C_{Di} with the already estimated zero-lift drag C_{D0} leads to the total drag coefficient C_D .

Subsequent to the *Advanced Aerodynamics* design step, the value of the maximum take-off mass is updated with the OEM and fuel mass estimated in the *Component Mass Estimation* and *Mission Performance* steps. If the new maximum take-off mass shows a difference to the previous value greater than a predetermined delta, then consequently the third iteration loop is started. During this, the *Point Performance* to *Advanced Aerodynamics* design steps (with the exception of the *Airfoil Selection* design step) are executed - the *Mission Performance* step with updated aerodynamic data. After the third iteration loop converged, constraints (e.g. wingspan) are checked in a final design step. If this is not the case, a valid converged design is presented to the user.

4. RESULTS AND DISCUSSION

In the following, the implemented methods presented in the previous sections are validated through the exemplary design of a General Dynamics F-16A Block 15 Fighting Falcon military aircraft. First, the reference aircraft is presented. Second, the ADEBO design schedule's resulting values are compared with the corresponding values of the reference aircraft and discussed. In the latter subsection, the outlier differences are presented and analysed.

4.1. Reference Aircraft F-16A

The F-16A is a multi-role fighter with high manoeuvrability and equipped with a single engine. It is capable of supersonic flight up to Mach 2. It was the first production fighter to be designed with unstable static stability in certain points of its flight envelope. Due to the shift of its aerodynamic center the configuration becomes stable in the supersonic flight regime. The wing of the F-16A has a cranked wing layout with wing-fuselage blending for increased aerodynamic performance. The fore-body strakes create a vortex system enabling higher angles of

attack during manoeuvring. As for the engine, the F100-PW-220 with its high maximum thrust was installed on the F-16A.

The F-16A Block 15 has been selected for validation. The collected initial assumptions of geometric, aerodynamic, and mass properties for this version are summarized in TABLE 2 and a three-view of the aircraft is shown in FIGURE 6. Since a plain flap system is installed on the leading and the trailing edge of the F-16, for the lift coefficient increase due to the high-lift system $\Delta C_{L_{HLD}}$ a value of 0.9 is assumed after [12]. Furthermore, the aircraft's maximum lift coefficient is determined to be 1.6 after [25].

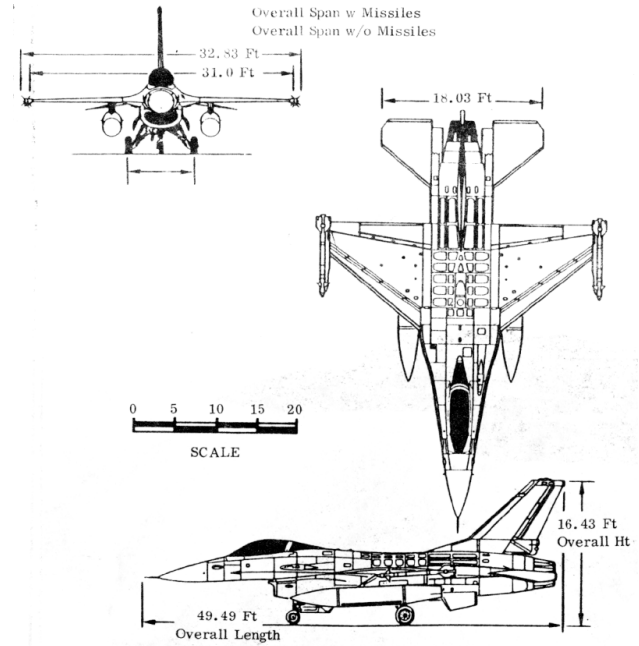


FIGURE 6. F-16A Block 15 three view adapted from [26]

TABLE 2. Initial assumptions for the F-16A fighter design (data from [12, 25–28])

Dimensions					
Wing		Horizontal Tail		Vertical Tail	
AR	3	AR	2.84	AR	1.28
λ	0.23	λ	0.22	λ	0.39
Λ_{LE}	40°	Λ_{LE}	40°	Λ_{LE}	40°

Mass and Propulsion			Aerodynamic Loads	
MTOM	16057 kg		$C_{L,max,plain}$	1.6
MLM	8845 kg		$\Delta C_{L,HLD}$	0.9
TSFC	$3.11 \cdot 10^{-5} (kg/s)N$		$n_{z,ult,+}$	13.2
TSFC _{AB}	$7.36 \cdot 10^{-5} (kg/s)N$		$n_{z,ult,-}$	-4.5
BPR	0.63			

The performance requirements of the *Point Performance* step are listed in TABLE 8 in the Appendix. Both the turn rate and specific excess power with their maximum achievable values are taken from the Standard Aircraft Characteristics for the F-16A Block 15.

For the estimation of the fuel mass required for the mission, a detailed description of the mission profile has to be provided. Following the division into different phases after Roskam [14], the aircraft is required to fly a mission in accordance with a typical air-to-ground mission with the applicable maximum combat radius of the F-16A adapted from [26]. After the take-off and climb section, the mission is divided into three main segments: The first (cruise) segment is flown at the subsonic Mach number of 0.85 for a distance of 611 km at an altitude of 10.4 km. This is followed by a combat manoeuvring phase with afterburner for 1.5 km consisting of the following elements:

- 1) Two energy exchanges of ΔE_s 12000 ft at Mach 0.85
- 2) One 360° 4g turn
- 3) Ammunition expanding resulting in a 2150 kg drop of payload
- 4) Energy exchange for the egress of ΔE_s 40000 ft and Mach 0.9
- 5) Return climb to cruise altitude

This is followed by a return cruise flight to the base and, prior to descend, by a loiter of 20 min duration.

4.2. Re-design of the F-16A

The design schedule converges to a maximum take-off weight of 16077 kg. The resulting intersecting design point in the design chart is found at a thrust-to-weight ratio of 1.06 and a wing loading of 5.29 kN/m^2 . Compared to the reference aircraft with a thrust-to-weight ratio of 1.03 and a wing loading of 5.26 kN/m^2 , the thrust-to-weight ratio is 2.9% greater and the wing loading is 0.6% greater. These values imply that the implemented limiting equations and the input values from TABLE 2 approximate the actual aircraft's design point well.

In the following, the geometric, powerplant, mass, and aerodynamic data of the re-design and the reference aircraft are compared and discussed in more detail.

4.2.1. Geometry

The resulting geometry of the re-design compared to an original F-16A is shown in a top-view in FIGURE 7 and in a side-view in FIGURE 8. Although the wing's and fuselage's geometry is well matched to the reference design, the most apparent difference between the two geometries is the resulting reduced empennage area.

TABLE 3. Comparison of geometric characteristics (F-16A data from [26])

Parameter	F-16A	ADEBO	Diff.
Fuselage length [m]	14.54	14.43	-0.8%
Wingspan [m]	9.45	9.46	0.1%
Wing area [m ²]	29.96	29.81	-0.5%
Inner wing sweep [deg]	78.00	76.76	-1.6%
Outer wing sweep [deg]	40.00	39.85	-0.4%
Hor. tail area [m ²]	13.01	9.81	-24.6%
Ver. tail area [m ²]	5.72	3.94	-31.1%

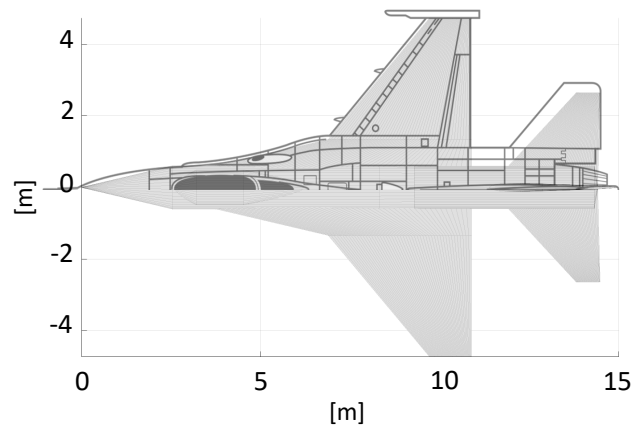


FIGURE 7. Top-view of the resulting re-design within ADEBO

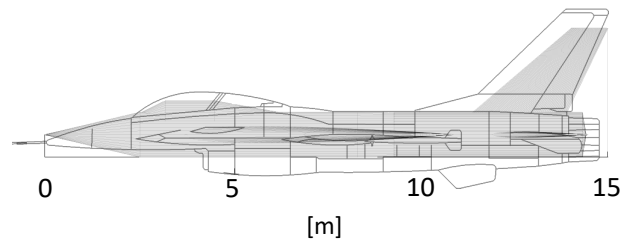


FIGURE 8. Side-view of the resulting re-design within ADEBO

As stated above, comparing the estimated vertical stabilizer area to the reference data, one can see the largest difference of the re-design compared to the reference aircraft. However, this underestimation reflects the actual F-16's conceptual tail design which had to be extended to provide sufficient directional stability in high angle of attack flight conditions [19]. The second largest difference in the re-design concerns the horizontal stabilizer area. This can be explained by an increase of the horizontal stabilizer area from the F-16A Block 1-10 to the F-16A Block 15 by 35.7%, as can be deduced from [26]. This change was made due to the addition of two hardpoints under the air inlet chin impacting the center of gravity of the aircraft and thereby its stability requiring a higher horizontal stabilizer area [29]. Compared to the older F-16 variant, the estimated value is higher, as can be seen in TABLE 4.

TABLE 4. Comparison of horizontal tail areas (data from [26])

Hor. tail area [m ²]	F-16A	ADEBO	Diff.
F-16A Block 15	13.01	9.81	-24.6%
F-16A Block 1-10	9.59	9.81	6.25%

The difference in the wing area is negligibly small, namely -0.5%, because of the well-matched design point as

stated above. For the re-design, the selected airfoil from the method by Sadraey is the NACA 63-006. This airfoil is 2% thicker compared to the 4% of the NACA 64A204 profile used in the reference design [30]. As can be seen on the fourth digit, the actual aircraft's airfoil had camber, while a symmetrical airfoil was selected within this study. The slightly higher MTOM of the re-designed aircraft might imply the shift in the look-up table. Additionally, since the look-up table's "axis"-values are limited to whole decimal values, the re-designs resulting small ideal lift coefficient was rounded to 0 instead of 0.1. Furthermore, it has to be mentioned that the unique airfoil of the original F-16's is not listed among the selectable profiles of the look-up table.

In case of the fuselage length, the adjusted statistical equation of Raymer [2] results in a shorter fuselage by -0.8% only. The discussion of the fuselage's cross sectional deviation is excluded due to the simplified fuselage design.

4.2.2. Powerplant

In TABLE 5, the F-16A Block 15 aircraft's installed Pratt and Whitney F100-PW-220 jet engine's performance and geometrical values are compared with ADEBO's estimation.

TABLE 5. Comparison of engine characteristics (F100-PW-220 data from [26, 27])

Parameter	F100-PW-220	ADEBO	Diff.
Mass [kg]	1456	1367	-6.3%
Thrust AB [kN]	105.98	110.62	4.4%
TSFC _{sub} [(kg/s)N]	3.11	2.96	-4.8%
BPR [–]	0.63	0.63	0%
Length [m]	4.98	5.02	0.8%
Diameter [m]	1.18	1.19	0.8%

As presented in Section 3.2.4, the values are a result of Raymer's preliminary engine sizing method [2]. The 4.4% higher afterburner thrust is the direct result of the slightly higher thrust-to-weight ratio from the design chart. Furthermore, since the resulting subsonic cruise TSFC is smaller than the initially assumed one, it is used in consecutive calculations and the bypass ratio input is left unaltered. The well-matched engine dimensions show that Raymer's statistics-based equations lead to reasonable results.

4.2.3. Masses

During the design process, the payload was assumed to be $\approx 5.2 t$ [26]. Included in the payload are all externally mounted masses. These include, but are not limited to, missiles, rockets, bombs, external fuel tanks and their fuel, and various pods. The assumed crew mass was estimated to be $100 kg$. Furthermore, the component mass breakdown of structure, propulsion, and fixed masses is close to the reference aircraft as well, deviating by a maximum of 2% , as can be seen in TABLE 6.

TABLE 6. Comparison of mass breakdown (F-16A data from [26])

Component	F-16A	ADEBO	Diff.
Structure	45%	46%	1%
Propulsion	29%	27%	2%
Fixed	26%	27%	1%

After the last iteration loop, as result of the accurate component mass estimation, the OEM deviates by only 0.2% from the reference value. The resulting MTOM is well matched as well, with a difference to the reference value of 0.1% (see TABLE 7).

TABLE 7. Comparison of overall mass characteristics (F-16A data from [26])

Parameter	F-16A	ADEBO	Diff.
MTOM [kg]	16057	16077	0.1%
OEM [kg]	7572	7592	0.2%

4.2.4. Aerodynamics

To be able to judge the fidelity of the estimated lift and drag coefficient a reference source was consulted. A reference providing a wide range of aerodynamic data of the F-16B is [31]. The F-16B is a two-seater version of the F-16A. It was decided to compare with the F-16B data despite the differences between the F-16A and F-16B, because of their geometric similarity in overall layout with the only major difference being the elongated canopy.

In FIGURE 9, the lift coefficient for the F-16B and the ADEBO re-design at $Ma = 0.8$ can be seen. As range for the angle of attack α at $Ma = 0.8$, 0° to 25° was chosen. Comparing the lift coefficients of the F-16A re-design with the reference data, a divergence can be seen in the estimation for $Ma = 0.8$ in FIGURE 9. This diversion can be explained, with the fact that the currently implemented aerodynamic estimation methods are unable to account for dynamic controlled leading and trailing edge flaps as installed on the F-16A. However, with increasing angle of attack, the diversion shrinks as the effectiveness of the flaps reaches its peak and the non-linear lift effects begin to dominate the lift coefficient in the higher angle of attack range.

In FIGURE 10, the lift coefficient for the F-16B and the ADEBO re-design at $Ma = 2$ can be seen. As range for the angle of attack α at $Ma = 2$, 0° to 8° was chosen. The flown angle of attack range at high speeds is lower due to airframe and g-loading restrictions. The lift coefficient at $Ma = 2.0$, as can be seen in the figure, is nearly a recreation of the reference data.

In FIGURES 11 and 12, the drag coefficient of the F-16B and of the ADEBO re-design at $Ma = 0.8$ and $Ma = 2$ can be seen, respectively. The angle of attack ranges are the same as chosen for the lift coefficient. When comparing the estimated drag coefficients to the reference data,

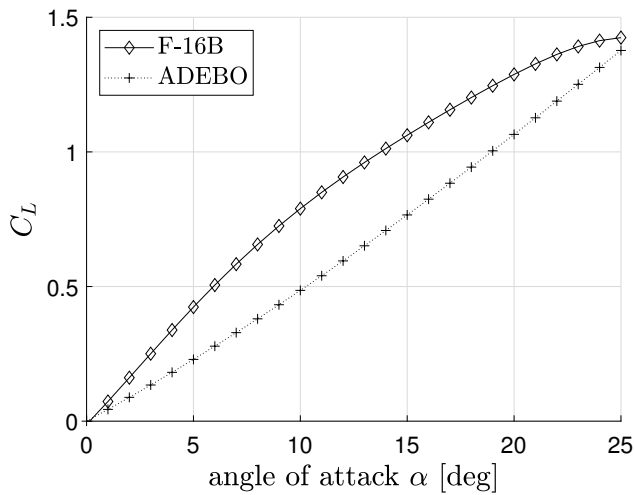


FIGURE 9. Lift coefficient at Mach = 0.8

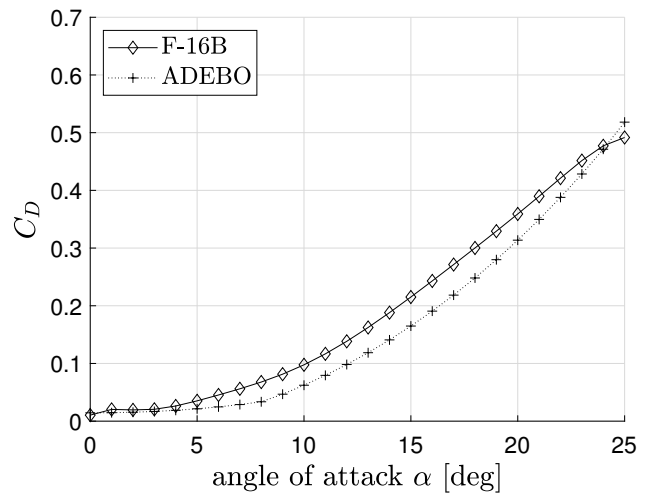


FIGURE 11. Drag coefficient at Mach = 0.8

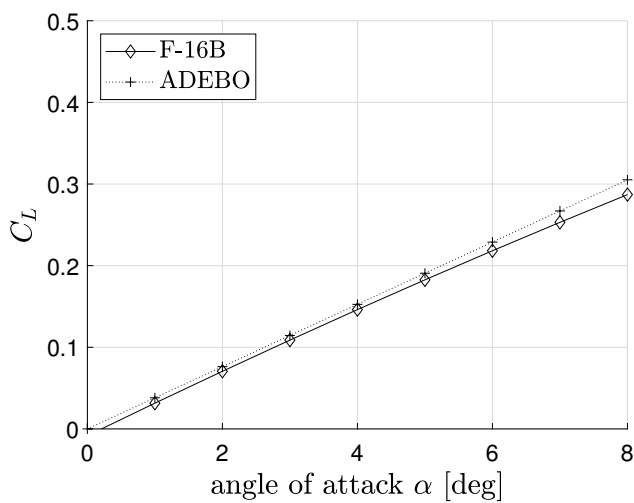


FIGURE 10. Lift coefficient at Mach = 2

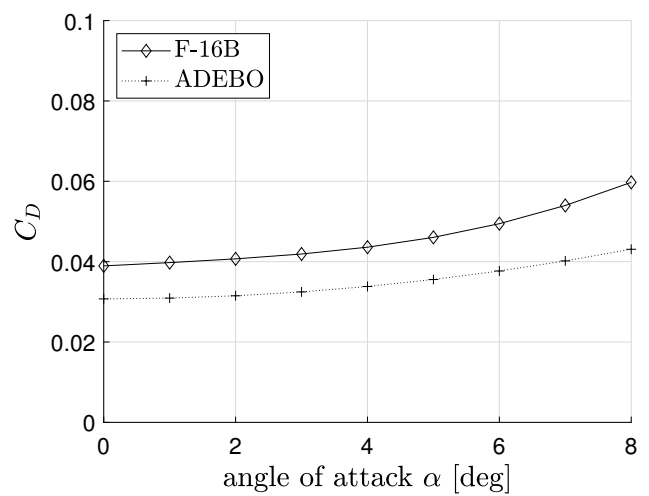


FIGURE 12. Drag coefficient at Mach = 0.8

one must consider that the drag coefficients of the F-16B data contain an increased value for the zero-lift drag as it carried two 370 gal external tanks and two AIM-9L Sidewinder air-to-air missiles. The ADEBO values consider a clean aircraft configuration without external payload.

Looking at the estimated drag at $Ma = 0.8$, a discrepancy of a maximum of $\Delta C_D = 0.05$ can be seen, but the general estimation of the drag coefficient matches well. Due to the higher resolution on the y-axis, the drag increase due to the external stores is more clearly visible in the $Ma = 2$ figure. The estimated drag coefficient matches the reference data fairly well.

It has to be pointed out that despite the $\frac{t}{c}$ ratio of the re-designed aircraft being 2% higher compared to the reference airfoil, the re-designed C_D are sufficiently accurate. This difference in thickness-to-chord ratio influences the critical lift coefficient $C_{L_{cr}}$, as can be seen in EQUATION 15, which again influences the choice of calculation method for the induced drag C_{Di} , as can be seen in TABLE 1.

5. CONCLUSION AND FUTURE WORK

Enhancing ADEBO to design a fighter aircraft was successful: The main aircraft parameters, which can be determined in aircraft conceptual design could be estimated adequately. The geometric properties of the reference aircraft were matched closely. The encountered differences in the horizontal and vertical tail area of the aircraft were explainable as result of modifications made to the F-16A configuration after its conceptual design phase. The relevant masses could also be estimated very well. The re-design of the engine was successful with the main discrepancy being its lower mass. Nonetheless, the thrust specific fuel consumption with afterburner could not be estimated and was adopted from [27]. Concerning the estimation of the aerodynamic characteristics, the implemented method developed by Paniszczyn and Staudacher proved to be a valuable tool and resulted in a fairly accurate estimation of the reference aircraft's lift and drag characteristics. The remaining disparities can be attributed to the missing modelling of the dynamic leading and trailing edge flap system.

To further enhance ADEBO's fighter design capabilities, several additions to the fighter design schedule are planned. The already mentioned problem of estimating

the TSFC of an afterburning engine will be tackled by connecting the GasTurb software to the fighter design schedule. Furthermore, it is planned to integrate the ability to consider thrust vectoring capabilities. Additionally, it is envisaged to enhance ADEBO's capabilities with respect to modelling the fuselage including basic radar stealth principles. This task could be achieved by using OpenVSP, a program used for this task in the METU fighter design process. Another foreseen improvement is to integrate a more detailed modelling for under-wing and under-fuselage payload. For example, the detailed DATCOM method could be integrated for the estimation of the increase of zero-lift drag resulting from store mounting. A core element to be added to the fighter design schedule is the implementation of primary and secondary control surfaces. As a possible result, the gap between the reference and estimated lift coefficient due to dynamic control of leading and trailing edge flaps might be closed. Lastly, the implementation of methods to estimate the overall combat performance of an resulting aircraft configuration is considered. A viable candidate for integration might be the combat effectiveness methodology developed by Kitowski, which considers sustainability, lethality, survivability, and affordability [32].

REFERENCES

- [1] D. P. Raymer. RDS - A PC-Based Aircraft Design, Sizing, and Performance System. In *Guidance, Navigation and Control Conference*, Reston, Virginia, United States of America, 08101992. American Institute of Aeronautics and Astronautics. DOI: [10.2514/6.1992-4226](https://doi.org/10.2514/6.1992-4226).
- [2] D. P. Raymer. *Aircraft Design: A Conceptual Approach*. American Institute of Aeronautics and Astronautics, 2012. ISBN: 9781600869112. DOI: [10.2514/4.104909](https://doi.org/10.2514/4.104909).
- [3] DARcorporation. *Advanced Aircraft Analysis - Aeronautical Design Software*, 2021.
- [4] J. A. Schwartz. *Fighter Aircraft Design System User's Manual*. Technical Report IDA Memorandum Report M-430, Institute for Defense Analysis, Alexandria, Virginia, United States of America, 1988.
- [5] M. L. Cramer. *Microcomputer Software Support for Classes in Aircraft Conceptual Design*. Master Thesis, Naval Postgraduate School, Monterey, United States of America, 1987.
- [6] M. Tokel. *Conceptual Design Synthesis of Fighter Aircraft*. Master Thesis, Middle East Technical University, Kızılay, Ankara, Turkey, 2019.
- [7] Department of Defense. MIL-STD-3013: Glossary of Definitions, Ground Rules, and Mission Profiles to Define Air Vehicle Performance Capability, 2 2003.
- [8] S. A. Brandt. The Effect of Initial Engine Sizing on Fighter Aircraft Final Optimized Size and Cost. In *2018 Aviation Technology, Integration, and Operations Conference*, Reston, Virginia, 2018. American Institute of Aeronautics and Astronautics. DOI: [10.2514/6.2018-3834](https://doi.org/10.2514/6.2018-3834).
- [9] H. Feng, M. Luo, H. Liu, and Z. Wu. A Knowledge-Based and Extensible Aircraft Conceptual Design Environment. *Chinese Journal of Aeronautics*, 24(6):709–719, 2011. DOI: [10.1016/S1000-9361\(11\)60083-6](https://doi.org/10.1016/S1000-9361(11)60083-6).
- [10] S. Herbst. *Development of an Aircraft Design Environment Using an Object-Oriented Data Model in MATLAB*. PhD thesis, Technical University of Munich, Munich, Germany, 2018.
- [11] S. A. Varga. *Enhancement of an Aircraft Design Environment for the Design of Fighter Aircraft and Validation through an Exemplary Fighter Design*. Master Thesis, Technical University of Munich, Munich, Germany, 2019.
- [12] M. H. Sadraey. *Aircraft Design: A Systems Engineering Approach*. John Wiley & Sons Ltd, 2013. ISBN: 9781119953401.
- [13] M. Hornung. Lecture Notes "Aircraft Design", 2017.
- [14] J. Roskam. *Airplane Design Part I: Preliminary Sizing of Airplanes*. Airplane Design. DARcorporation, 2018. ISBN: 97818848855426.
- [15] T. R. Sieron, D. Fields, A. W. Baldwin, and D. W. Adamczak. *Procedures and Design Data for the Formulation of Aircraft Configurations*. Technical report, Wright Laboratory, AFMC, Wright Patterson AFB, Dayton, Ohio, United States of America, 1993.
- [16] J. Roskam. *Airplane Design Part VI: Preliminary Calculation of Aerodynamic, Thrust and Power Characteristics*. Airplane Design. DARcorporation, 1987. ISBN: 1884885527.
- [17] R. D. Finck. USAF (United States Air Force) Stability and Control DATCOM (Data Compendium). Technical report, MCDONNELL AIRCRAFT CO, ST LOUIS, St. Louis, Missouri, United States of America, 1978.
- [18] LTH. *Luftfahrttechnisches Handbuch*, 2015.
- [19] M. Hornung. Lecture Notes "High Performance Aircraft", 2020.
- [20] J. Roskam. *Airplane Design Part V: Component Weight Estimation*. Airplane Design. DARcorporation, 2019. ISBN: 9781884885501.
- [21] F. A. Woodward, R. Carmichael, A. Kawaguchi, E. Tinoco, J. Larsen, and R. Wallace. *NASA Ames Wing Body Panel Program*, 1959.

- [22] W. Staudacher. *The Influence of Leading Edge Vortex Systems of Slender Wings [Die Beeinflussung von Vorderkantenwirbelsystemen schlanker Tragflügel]*. PhD thesis, Stuttgart University, Stuttgart, Germany, 1992.
- [23] T. F. Paniszczyn. Prediction of Lift and Aerodynamic Center for Variable Sweep Wings. In *5th Aerospace Sciences Meeting*, page 135, New York, United States of America, 1967. DOI: [10.2514/6.1967-135](https://doi.org/10.2514/6.1967-135).
- [24] E. C. Polhamus. A Concept of the Vortex Lift of Sharp-Edge Delta Wings Based on a Leading-Edge-Suction Analogy. Technical Report TN D-3767, NASA Langley Research Center, Langley Station, United States of America, 1966.
- [25] L. T. Nguyen, M. E. Ogburn, W. P. Gilbert, K. S. Kibler, P. W. Brown, and P. L. Deal. Simulation Study of Stall/Post-Stall Characteristics of a Fighter Airplane with Relaxed Static Stability. Technical Report NASA-TP-1538, NASA Langley Research Center, Hampton, Virginia, United States of America, 1979.
- [26] Department of the Airforce. USAF Standard Aircraft Characteristics: AFG 2, Vol-1, Addn 58. Technical report, US Department of the Airforce, Washington, DC, United States of America, 1984.
- [27] L. M. Nicolai and G. Carichner. *Fundamentals of Aircraft and Airship Design*. AIAA educational series. American Institute of Aeronautics and Astronautics, Reston, United States of America, 2010. ISBN: 9781600867514. DOI: [10.2514/4.867538](https://doi.org/10.2514/4.867538).
- [28] US Department of the Airforce. Military Specification, Standard Aircraft Characteristics and Performance, Piloted Aircraft, MIL-C-005011B. Technical report, US Department of the Airforce, Washington, DC, United States of America, 1977.
- [29] E. Hehs. History Of The F-16 Fighting Falcon. *CODE ONE*, 12(3), 1997.
- [30] M. C. Fox. *Supersonic Aerodynamic Characteristics of an Advanced F-16 Derivative Aircraft Configuration*, volume 3355. NASA, 1993.
- [31] G. L. Beeker, R. L. Bennet, and J. L. Payne. *Volume 1 Performance Flight Testing: Chapter 14 Aerodynamic Modeling*. United States Airforce, Edwards Air Force Base, United States of America, 1996.
- [32] J. Kitowski. Combat Effectiveness Methodology as a Tool for Conceptual Fighter Design. In *Aerospace Design Conference*, page 1197, 1992. DOI: [10.2514/6.1992-1197](https://doi.org/10.2514/6.1992-1197).

APPENDIX

TABLE 8. Performance requirements for the F-16A fighter design schedule adapted from [26]

Distance Roll (Take-Off)		Distance Roll (Landing)	
Altitude	0 <i>m</i>	Altitude	0 <i>m</i>
Manoeuvring Mass	15800 <i>kg</i>	Manoeuvring Mass	12473 <i>kg</i>
Distance Roll	762 <i>m</i>	Distance Roll	905 <i>m</i>
Sustained Turn Rate (STR)		Attained Turn Rate (ATR)	
Altitude	4572 <i>m</i>	Altitude	4572 <i>m</i>
Velocity	274 <i>m/s</i>	Velocity	274 <i>m/s</i>
Manoeuvring Mass	10460 <i>kg</i>	Manoeuvring Mass	10780 <i>kg</i>
STR	12 °/s	ATR	18 °/s
Maximum Mach Number		Specific Excess Power (SEP)	
Altitude	11000 <i>m</i>	Altitude	4572 <i>m</i>
Mach Number	1.8	Velocity	274 <i>m/s</i>
Manoeuvring Mass	10460 <i>kg</i>	Manoeuvring Mass	10781 <i>kg</i>
		SEP	182 <i>m/s</i>
Stall Speed		Required Average Mach Cruise	
Altitude	0 <i>m</i>	Mach Number	0.8
Manoeuvring Mass	15866 <i>kg</i>	Required Payload	
Stall Speed	59 <i>m/s</i> ^[12]	Payload Mass	5200 <i>kg</i>